Author's personal copy

Available online at www.sciencedirect.com

SciVerse ScienceDirect

Acta Materialia 60 (2012) 4336–4348

www.elsevier.com/locate/actamat

Rate-dependent behavior of Sn alloy–Cu couples: Effects of microstructure and composition on mechanical shock resistance

K.E. Yazzie [a], H.E. Fei [b,1], H. Jiang [b], N. Chawla [a,b,*]

[a] Materials Science and Engineering, School for Engineering of Matter, Transport, and Energy, Arizona State University, Tempe, AZ 85287-6106, USA
[b] Mechanical and Aerospace Engineering, School for Engineering of Matter, Transport, and Energy, Arizona State University, Tempe, AZ 85287-6106, USA

Received 25 March 2012; received in revised form 10 April 2012; accepted 11 April 2012
Available online 19 May 2012

Abstract

Solders serve as electrical and mechanical interconnects in electronic packaging. The mechanical shock behavior of a Pb-free solder joint is quite complex, since the influences of solder microstructure, intermetallic compound (IMC) layer thickness, and strain rate on the overall dynamic solder joint strength need to be quantified. Dynamic solder joint strength is hypothesized to be controlled by two factors. At low strain rates it should be controlled by the bulk solder, whereas at high strain rates it may be controlled by the brittle intermetallic compound layer. In this paper, the dynamic solder joint strength of Sn–3.9 Ag–0.7 Cu solder joints was experimentally measured over the strain rate range 10^{-3}–12 s^{-1}. The influences of changes in solder microstructure and IMC layer on dynamic solder joint strength were quantified, and visualized in three dimensions. Fracture mechanisms operating in the solder-controlled and IMC layer-controlled dynamic strength regimes are discussed. Finally, qualitative numerical simulations were conducted, which accurately depict the experimentally observed fracture behaviors.
© 2012 Acta Materialia Inc. Published by Elsevier Ltd. All rights reserved.

Keywords: Pb-free solder; Mechanical shock; Fracture; Cu_6Sn_5; Strain rate

1. Introduction

Solders serve as electrical and mechanical interconnects in electronic packaging. The need to develop environmentally benign electronic packages has generated great interest in Pb-free solder alloys [1–6]. Performance demands placed on advanced electronic packages dictate that an increasing number of solder interconnects be built into increasingly smaller spaces. As electronic packages are made smaller for portable devices, there is an increased probability that solder joints may fail by accidental dropping during manufacture, shipping, or use. An understanding of the solder joint strength over a range of strain rates is needed, since the strain rates experienced by solders during drop, i.e. mechanical shock, are in an intermediate range between quasi-static and dynamic regimes, i.e. between 10^{-1} s^{-1} and 10^{2} s^{-1} [7–13].

Pb-free solders are Sn-rich, with small alloying additions of Ag and/or Cu. Above the eutectic melting point the alloying additions react with the Sn to form Ag_3Sn and Cu_6Sn_5 precipitates that serve as barriers to dislocation motion, thereby strengthening the solder [3]. The bulk solder microstructure of Sn-based alloys containing Ag or Cu consists of Sn-rich dendrites surrounded by a eutectic mixture of Ag_3Sn and Cu_6Sn_5, and is determined largely by the cooling rate [14,15]. When solder joints are fabricated the Sn-based alloy is melted over a metallization layer, such as Cu or Ni. From the reaction between Sn and Cu, a Cu_6Sn_5 intermetallic compound (IMC) layer is formed at the solder/Cu interface. Several studies have been conducted on the mechanical shock behavior of Sn-based

* Corresponding author at: Fulton Professor of Materials Science and Engineering, School for Engineering of Matter, Transport, and Energy, Arizona State University, Tempe, AZ 85287-6106, USA. Tel.: +1 480 965 2402; fax: +1 480 727 9321.
E-mail address: nchawla@asu.edu (N. Chawla).
[1] Present address: Intel Corp., 5000 W. Chandler Blvd, Chandler, AZ 85226, USA.

1359-6454/$36.00 © 2012 Acta Materialia Inc. Published by Elsevier Ltd. All rights reserved.
http://dx.doi.org/10.1016/j.actamat.2012.04.018

Author's personal copy

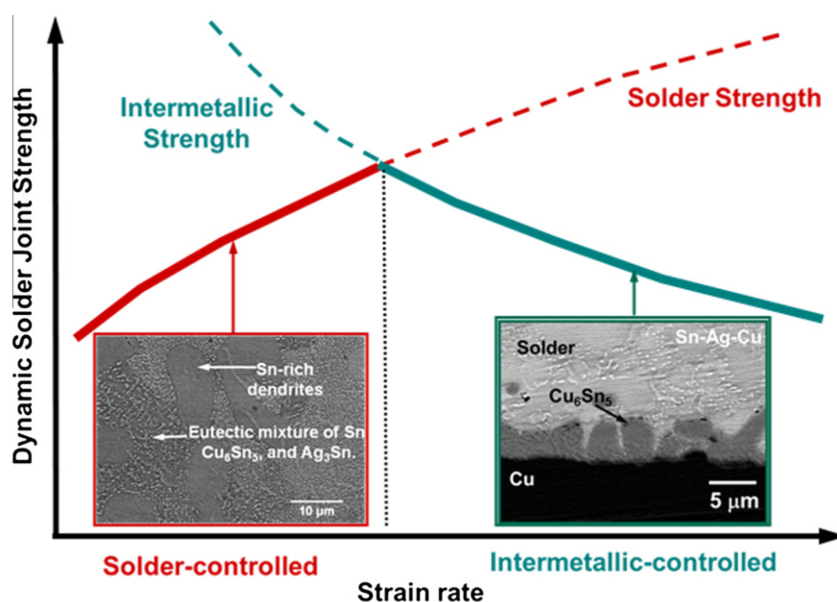

Fig. 1. Schematic showing the dynamic solder joint strength to be controlled by bulk solder strength at low strain rates and by strength of intermetallic layer at high strain rates [1].

solder joints, although a precise understanding of the mechanisms of deformation, particularly as a function of strain rate, is still needed [11,12].

The mechanical shock behavior of Sn-rich alloys bonded to the Cu substrate by the Cu_6Sn_5 layer is quite complex [16–18]. It has been hypothesized that the solder joint behavior is strain-rate-dependent, being controlled by either the solder or the IMC layer. A schematic representation of this behavior is shown in Fig. 1 [1]. At lower strain rates the strength is controlled by the ductile deformation of the solder, which increases with strain rate due to strain rate hardening [19]. At high strain rates it is controlled by the strength of the IMC layer, because the stress in the Sn becomes highly triaxial with very little time for stress relaxation, and brittle fracture localized in the intermetallic layer dominates [20]. Indeed, Cu_6Sn_5 is known to have a much larger Young's modulus than Sn-rich solder [21], and it fractures in a brittle manner [22]. A maximum dynamic solder joint strength occurs at a critical transition strain rate where both fracture mechanisms have equal contributions. More importantly, we hypothesize that changes in the solder microstructure and IMC layer thickness will cause shifts of the dynamic solder joint strength curve. Preliminary experiments tend to support this trend [23]. A fundamental understanding of the dynamic solder joint strength requires quantification of the relationship between solder-controlled and IMC-controlled mechanical properties [20,24,25].

To understand the relationship between the intermetallic layer and mechanical shock resistance, it is necessary to conduct systematic experiments where: (a) the intermetallic layer thickness is held constant while the solder microstructure is changed, and (b) the intermetallic layer thickness is varied while the solder microstructure (and strength) is held constant. Experiments of type (a) can be conducted by isothermally aging solder joints at low temperature, which coarsens solder microstructure while maintaining a relatively constant IMC layer thickness. Experiments of type (b) can be conducted by holding solder joints in extended reflow, i.e. when the Sn is molten over long periods of time in contact with Cu, which grows the IMC layer. Here the solder microstructure is kept constant since it is controlled by a constant cooling rate [26,23]. This approach enables accurate characterization of the mechanical shock behavior of the solder joints with the ability to isolate the effects of solder microstructure and intermetallic layer.

In this paper, the relationship between solder microstructure and intermetallic layer thickness with the dynamic solder joint strength was systematically quantified over the strain rate range 10^{-3} s^{-1} to 12 s^{-1}. The transition from solder-controlled to IMC layer-controlled fracture was characterized. The effect of solder yield strength and IMC layer thickness on dynamic strength was also quantified, to validate hypotheses about the relationship between solder microstructure and dynamic solder joint strength. It will be shown that, at lower IMC thickness the hypothesis of a transition from solder-controlled to IMC layer-controlled fracture is true. At larger IMC thickness, however (~20 μm) the behavior is IMC layer-controlled at all strain rates tested. Fracture mechanisms operating in solder-controlled and IMC layer-controlled regimes were characterized. Finally, qualitative finite element method (FEM) simulations of solder joint deformation were conducted at various strain rates with varying IMC layer thicknesses. The fracture behavior observed in the FEM simulations agreed well with that observed experimentally.

Author's personal copy

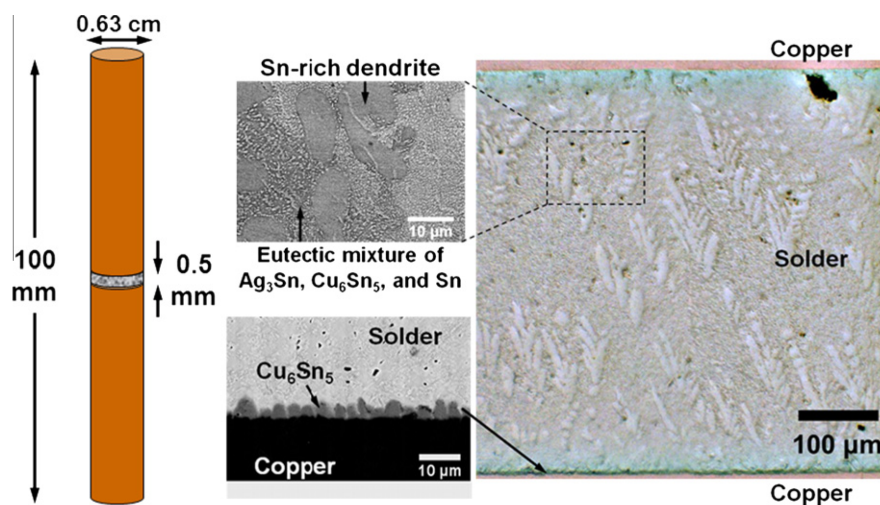

Fig. 2. Joint geometry and microstructural characterization of as-reflowed Sn–3.9 Ag–0.7 Cu solder joint. Optical micrograph showed microstructure consisting of Sn-rich dendrites and eutectic mixture of Sn, Ag_3Sn, and Cu_6Sn_5. Backscatter SEM micrograph showed thickness and nodular morphology of Cu_6Sn_5 intermetallic layer.

2. Materials and experimental procedure

Sn–3.9 Ag–0.7 Cu solder (Indium Corp., Utica, NY, USA) was reflowed between two oxygen-free high-conductivity (OFHC) copper bars (25 mm long and 6.35 mm diameter) to form butt joints. Copper bars were mechanically polished to a 0.05 μm colloidal silica finish. A mildly activated rosin flux was then applied to the end of the copper bars to promote wetting between the solder and Cu during reflow. A jig was used to create a reproducible joint thickness of 500 μm, as shown in Fig. 2. The jig and solder joints were heated on a programmable digital hot plate (Torrey Pines Scientific, San Marcos, CA, USA) until the solder reached its melting temperature. Temperatures during reflow and aging were measured using a thermocouple placed near the joint. As-reflowed solder joints were held for 40 s above the melting temperature, removed from the hot plate, and air-cooled on an aluminum block at $\sim$1 °C s^{-1}. As-reflowed solder joints were an experimental control against which the changes in microstructure and overall strength for the isothermally aged and extended reflow solder joints were compared. Isothermally aged solder joints were produced by aging as-reflowed solder joints at either 140 °C or 175 °C, for 24, 72, and 500 h. Extended reflow solder joints were heated to a nominal reflow temperature of 230 °C, and then held at that temperature for 3, 24, and 168 h.

Optical microscopy and scanning electron microscopy (SEM, FEI-XL30) were used to characterize the solder joint microstructure and perform fractography. Average intermetallic layer thickness was computed with at least 500 measurements from SEM micrographs. The measurements were made by segmenting backscattered SEM micrographs to isolate the IMC layer. Then a series of 1 pixel-wide lines was mathematically subtracted from the segmented images of the IMC layer using ImageJ (NIH, Bethesda, MD, USA). The result was an image of 1 pixel-wide lines whose height corresponded to the thickness of the IMC layer. The height of the line segments was then measured using ImageJ's particle analysis tool. Average Vickers microhardness was computed from 10 measurements taken at 72.8 gf with a hold time of 15 s.

Tensile tests were conducted on solder joints, over the range of strain rates 10^{-3}–12 s^{-1}, using an MTS 810 servo-hydraulic machine. Tests were conducted in strain control at 10^{-3} and 10^{-1} s^{-1} using an extensometer. Tests at 1.5, 3, and 12 s^{-1} were conducted in displacement control. A slack adapter was utilized to ensure that a well-controlled, linear strain rate was achieved. To prevent damage, an extensometer was not used at these higher strain rates. Instead, a small section of the joint was polished to a 0.05 μm colloidal silica finish to permit visualization of the joint interfaces. A Questar QM100 (New Hope, PA, USA) traveling microscope was used in conjunction with a Phantom Miro2 (Wayne, NJ, USA) high speed camera to measure strain from the displacement of the joint interfaces. Energy dispersive X-ray spectroscopy (EDS) was used to identify the composition of the IMC layer and precipitates on the fracture surfaces.

3. Results and discussion

3.1. Microstructural characterization

Fig. 2 shows a representative microstructure of the as-reflowed solder joints, which consisted of Sn-rich dendrites surrounded by a eutectic mixture of Ag_3Sn and Cu_6Sn_5 precipitates. A relatively thin, nodular IMC layer was formed in the as-reflowed solder joints. Fig. 3 shows the solder microhardness for as-reflowed (0 h condition), isothermally aged, and extended reflow solder joints. As-reflowed solder joints had a solder microhardness of 113.9 ± 4.8 MPa. The solder microhardness of the isothermally aged solder joints decreased with aging time, due to coarsening of the solder

Author's personal copy

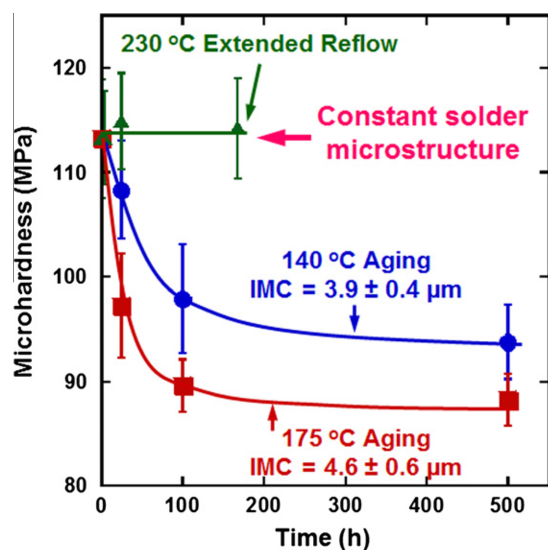

Fig. 3. Solder microhardness measured over treatment time for extended reflow and isothermally aged solder joints. As-reflowed solder joints had a microhardness of 113.9 ± 4.8 MPa. Extended reflow solder joints had nearly constant solder strength, equal to that of as-reflowed solder joints. Isothermally aged solder joints had decreasing solder strength. The microhardness of joints aged at 140 °C was always greater than joints aged at 175 °C. This technique produced solder joints in which the influence of solder strength (microstructure) was isolated.

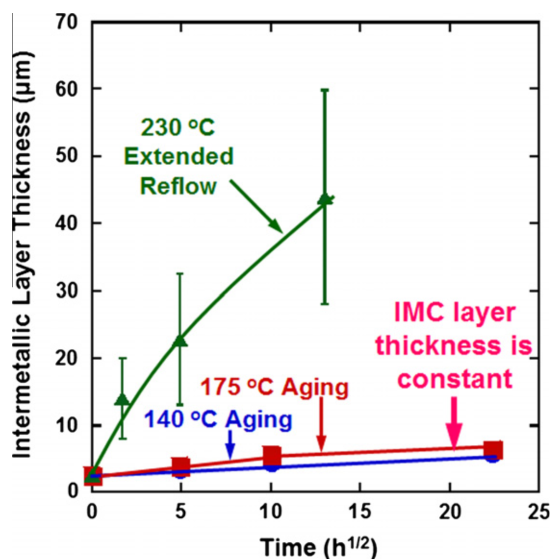

Fig. 4. IMC layer thicknesses measured over treatment time for extended reflow and isothermally aged solder joints. Isothermally aged solder joints had nearly constant IMC layer thickness. Extended reflow solder joints had an increasing IMC layer thickness. This technique produced solder joints in which the influence of IMC layer thickness was isolated.

microstructure, particularly Ag_3Sn and Cu_6Sn_5 precipitates, which reduced their effectiveness as dislocation barriers. The solder microhardnesses of joints aged at 175 °C were ~10 MPa lower than those of joints aged at 140 °C, due to the increased driving force for microstructural coarsening at higher temperature. The largest decrease in microhardness occurred approximately within the first 100 h of aging. After 100 h the rate of decrease in microhardness with aging time slowed. Extended reflow solder joints had constant solder microhardness of ~113 MPa, equal to that of the as-reflowed solder joints. The solder microhardness was kept constant by maintaining a constant solder microstructure, which was controlled using a constant cooling rate. Thus, two sets of solder joints were fabricated, with very different solder microstructures.

After the solder microhardness was quantified, the IMC layer thickness was measured. The average IMC layer thickness of the as-reflowed solder joints (0 h condition), was 2.5 ± 0.6 µm, as shown in Fig. 4. Isothermally aged solder joints showed only a slight increase in IMC layer thickness. The IMC layers grew to final average thicknesses of 5.6 ± 0.6 µm and 6.5 ± 0.4 µm, for aging for 500 h at 140 °C and 175 °C, respectively. It is clear that while isothermal aging at 140 °C and 175 °C produced significant differences in the solder microstructure and microhardness, there was no significant difference in the intermetallic layer thicknesses. Thus, low temperature isothermal aging essentially produced solder joints with constant IMC layer thicknesses, and significantly different solder microstructures, thereby providing a means to isolate the effect of solder microstructure.

During long periods of extended reflow time the bottom IMC layer would continue to grow while the top IMC layer reached a critical thickness after which the top IMC layer did not get any thicker [29]. This growth behavior was undesirable, since an asymmetric IMC layer thickness would promote non-uniform deformation within the solder joint. Therefore, a simple method of encasing the joint in a shaft collar and rotating the assembly at equal time intervals during extended reflowed was adopted. The rotation method produced uniform IMC layer thicknesses on both sides of the solder joint. The intermetallic layer thickness reported in Fig. 4 for extended reflow joints is based on measurements made on joints fabricated using the rotation method, and therefore having a symmetric IMC layer thickness on both sides of the joint. The average IMC layer thicknesses for as-reflowed solder joints, and solder joints held in extended reflow for 3, 24, and 168 h, were 2.5 ± 0.6 µm, 14.0 ± 5.9 µm, 22.8 ± 9.7 µm, and 44.0 ± 15.9 µm, respectively. During growth the IMC layer remained nodular, which may account for some of the standard deviations shown in Fig. 4. It is clear that extended reflow produced large changes in IMC layer thickness, while maintaining a constant solder microstructure. Conversely, isothermally aged solder joints maintained a constant IMC layer thickness, while producing large changes in solder microstructure. In this fashion, joints which isolated the effects of solder microstructure and IMC layer thickness were obtained.

3.2. Influence of solder microstructure on mechanical shock behavior (constant IMC layer thickness)

In this section we describe the deformation behavior of the solder joints. Strain in the solder joint was measured

Author's personal copy

using an extensometer for tests conducted at strain rates less than 1 s^{-1}. The gage length of the extensometer was larger (10 mm) than the gage length of the solder joint (500 μm). Therefore, the strain measured by the extensometer had to be corrected for the additional compliance of the copper bars, using the following equation [30]:

$$\varepsilon_{solder} = \left(\frac{1}{L_0}\right)\left(\Delta X - L_{Cu}\frac{\sigma}{E_{Cu}}\right) \quad (1)$$

where L_0 is the solder joint's original thickness, ΔX is the total displacement measured from the extensometer, σ is the tensile stress, L_{Cu} is the length of the copper bars (9.5 mm), and E_{Cu} was the elastic modulus of the OFHC Cu bar, taken to be 116 GPa [31].

Strain in the solder joint was measured using a high speed camera and Questar traveling microscope for strain rates greater than 1 s^{-1}. In this case strain was measured directly from the displacement of the Cu–solder–Cu interface observed from the high speed video, at up to 20,000 frames s^{-1}. Preliminary tensile tests at high strain rate showed a non-linear initial "lag" in the strain vs. time response of the solder joint. The lag corresponded to a displacement of ~90 μm. The reason for the lag was that the MTS 810 actuator could not accelerate fast enough to reach the specified displacement rate over the 90 μm distance, despite that fact that it was tuned to reach a high displacement rate as rapidly as possible. Indeed, the 90 μm lag would be negligible for a larger sample, but it was significant on the scale of the solder joint (500 μm). Therefore, a slack adapter was utilized with high strain rate experiments to ensure that the required linear strain rate was obtained during solder joint deformation. It did this by providing a free travel distance, allowing the actuator to reach a specified displacement rate, before engaging the solder joint. While a free travel distance of only 90 μm was needed, for practical purposes a distance of 1 cm was used. Fig. 5 shows that the final calibrations yielded strain rates that were linear and well-controlled.

Several studies have been performed to evaluate the strength of solder joints as a function of strain rate. They concluded that the solder strength and IMC layer strength both play important roles in determining the overall strength of the solder joint [32–34]. Furthermore, it was hypothesized that solder joint strength might change with variations in strain rate, solder microstructure, and IMC layer thickness, thereby constituting a dynamic solder joint strength. Other researchers have studied the effect of reflow conditions, solder composition, aging, and loading mode on the dynamic strength of solder joint arrays [35–37]. However, studies on solder joint arrays are more useful for quality control and design. Single solder joint test methods provide fundamental insight into the relationship between the complex stress state in solder joints during mechanical shock, with changes in solder microstructure and IMC layer thickness [1,25,26,23,38–40].

In this section we discuss the results of tensile tests conducted on single Sn–3.9 Ag–0.7 Cu solder joints, using the aforementioned techniques to isolate the effects of solder microstructure and IMC layer thickness. Ultimate tensile strength (UTS) values measured over a range of strain rates were plotted as a function of strain rate, as shown in Fig. 6. The green curve shown in Fig. 6a and b is the dynamic strength of as-reflowed solder joints. This curve was an experimental control against which all other trends in dynamic strength were compared. The dynamic strengths of as-reflowed solder joints increased monotonically from 45.6 ± 4.0 MPa to 75.4 ± 4.7 MPa in the strain rate range 10^{-3}–1.5 s^{-1}. This trend indicated the solder-controlled dynamic strength regime. The dynamic strengths of as-reflowed solder joints then decreased monotonically from 75.4 ± 4.7 MPa to 37.2 ± 10.9 MPa in the strain rate range 1.5–12 s^{-1}. This trend indicated the IMC layer-controlled dynamic strength regime.

The experimental results showed that the critical strain rate at which the dynamic solder joint strength transitioned from solder-controlled to IMC layer-controlled was at ~1 s^{-1}. Lal and Bradley [35] and Darveaux and Reichman [36] found that the transition strain rate of Sn–Ag–Cu solder joints was approximately in the range 10^{-2}–10^{-1} s^{-1}. They found that larger IMC layer thickness produced by multiple reflows, and stronger solders with higher wt.% of Ag and Cu, promoted brittle failure and decreased the transition strain rate. At the transition strain rate the stress state in the Sn in the solder joint is highly triaxial, and this begins to localize deformation at the IMC layer, due to the presence of stress concentrations at the IMC layer. Therefore, it should be expected that variations in solder joint geometry would cause changes in the triaxial stress state, thereby shifting the transition strain rate. Indeed, Zou and Zhang [39] found that solder joint strength was inversely proportional to joint thickness, due to the mechanical constraint imposed by thinner joint geometries. Their fractography showed that the mechanical constraint promoted brittle failure at the IMC layer in thinner joints, while thicker joints failed in a ductile manner.

It is clear that changes in solder microstructure may influence the dynamic solder joint strength. Therefore, the dynamic strengths for solder joints isothermally aged at 140 °C for 24, 72, and 500 h were measured, as shown in Fig. 6a. As aging time increased the solder microstructure coarsened with a commensurate decrease in the dynamic solder joint strength in the solder-controlled strength regime. The decrease was consistent with the decrease in solder microhardness shown in Fig. 3. Kumar et al. [41] measured the fracture toughness of Sn–3.8 Ag–0.7 Cu compact mixed-mode solder joints as a function of reflow time and aging over the strain rate range 10^{-2}–200 s^{-1}. They also observed a decrease in the fracture stress with decreasing solder microhardness, indicating more ductile fracture with decreasing solder strength. More importantly, since the IMC thickness is relatively the same, ~3.9 ± 0.4 μm in all our samples, the dynamic strengths in the IMC controlled regime were not affected by solder microstructure. Dynamic solder joint strength decreased

Author's personal copy

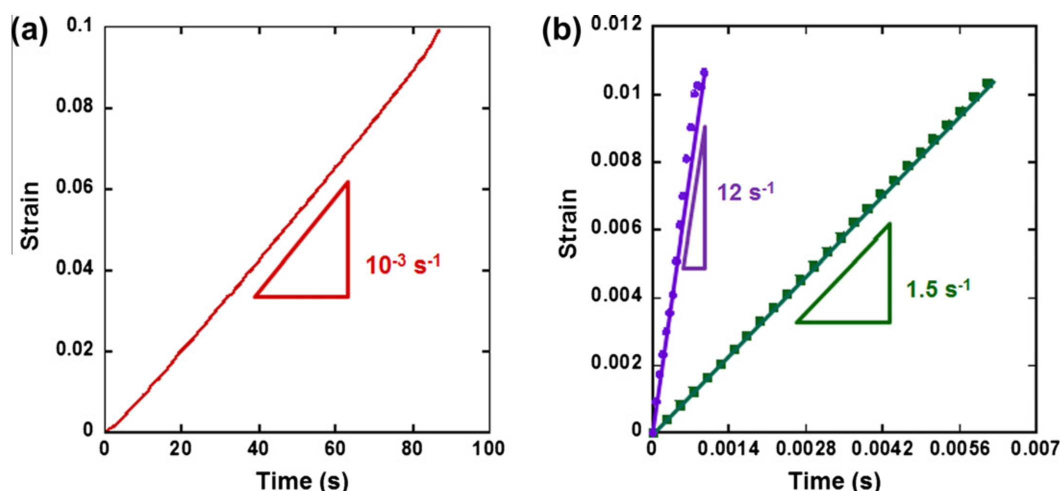

Fig. 5. Strain rates were well-controlled and linear. (a) Strain vs. time measured using extensometer. (b) Slack adapter was used with high strain rate tests. Strain vs. time measured from displacement of Cu–solder interface with Questar microscope and high speed camera.

in the IMC-controlled mode since the brittle IMC is sensitive to stress concentrations and flaws within the IMC layer [26,42,43]. Indeed, the IMC layer itself is known to serve as a site for stress concentration, which would increase with strain rate, thereby decreasing the overall strength of the joint.

The effect of higher isothermal aging temperature was also examined. Fig. 6b shows the dynamic strengths for solder joints isothermally aged at 175 °C for 24, 72, and 500 h. The higher aging temperature coarsened the microstructure more, compared to joints aged at 140 °C. Therefore, there was a larger decrease in the dynamic solder joint strength, for a given aging time and strain rate, in the solder-controlled strength regime. This was consistent with the larger decrease in solder microhardness shown in Fig. 3. Since the IMC layer thickness is relatively the same, 4.6 ± 0.6 μm in all the samples, the strengths in the IMC layer-controlled regime overlapped, irrespective of solder microhardness. The experimental results showed that the critical strain rate at which the joint strength transitioned from solder-controlled to IMC-controlled was at $\sim$1 s^{-1} for joints isothermally aged at 140 °C and 175 °C.

The influence of the solder microstructure and strain rate on the dynamic solder joint strength was visualized in three dimensions. Fig. 7a shows the dynamic solder joint strength plotted as a function of solder microhardness and strain rate for solder joints isothermally aged at 140 °C. This three-dimensional (3-D) representation of the data shows that the dynamic solder joint strength is a continuous function of solder microhardness and strain rate. The decrease in dynamic solder joint strength with decreasing solder microhardness is visible in the solder-controlled strength regime. The dynamic solder joint strength surface tends to be flatter in the IMC layer-controlled regime, reflecting the overlapping dynamic strengths produced by joints with constant IMC layer thickness. Fig. 7b shows the dynamic solder joint strengths plotted in 3-D for solder joints isothermally aged at 175 °C. The larger decrease in dynamic solder joint strength with decreasing solder microhardness is obvious in this plot, as the 3-D surface slopes downward in the solder-controlled strength regime. Here, again, the dynamic solder joint strength surface tends to be flatter in the IMC layer-controlled regime, reflecting the overlapping dynamic strengths produced by solder joints with constant IMC layer thickness. 3-D visualizations such as these are beneficial for designing robust solder joints, since, for instance, one can determine the peak strength for a given solder microhardness and strain rate. The 3-D visualization suggests that the peak solder joint strength could be tailored, for a given strain rate, by isothermally aging the solder joints. Indeed, they may also serve as valuable inputs for reliability models.

Kumar et al. [41] produced 3-D plots showing the fracture toughness as a function of effective IMC layer thickness and solder yield strength. In their plots, the fracture toughness slowly decreased, with increasing solder yield strength and IMC layer thickness. They noticed significant scatter when correlating the fracture toughness to the solder yield strength, and concluded that a third factor had to be taken into account, which was the IMC layer. Thus, a fundamental understanding of the influence of IMC layer thickness on dynamic solder joint strength needs to be quantified.

3.3. Influence of IMC layer thickness on mechanical shock behavior (constant solder microstructure)

The experimental results presented so far have been for solder joints with relatively thin and constant ($\leqslant$10 μm) IMC layer thicknesses. However, large IMC layer thickness has been shown to promote predominantly brittle fracture of the solder joint [26]. Lee et al. [42] observed that cleavage fracture through the IMC layer became dominant at an IMC layer thickness greater than 10 μm. Therefore, it is necessary to evaluate dynamic solder joint strength over a greater range of IMC layer thicknesses in order to see if

Author's personal copy

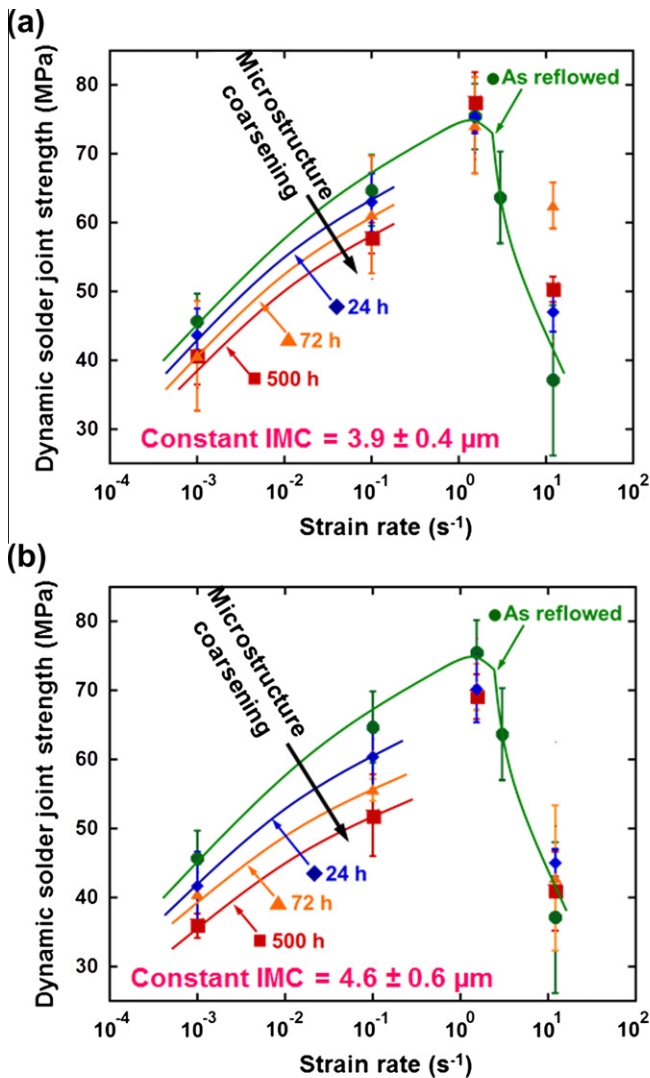

Fig. 6. UTS plotted as a function of strain rate for as-reflowed and isothermally aged solder joints showed the trend in solder-controlled and IMC-controlled dynamic strengths. (a) Dynamic strengths for solder joints aged at 140 °C decreased with aging time in the solder-controlled regime. (b) Dynamic strengths for joints aged at 175 °C decreased with aging time in the solder-controlled regime and were lower than strengths for solder joints tested at the same strain rate and aged at 140 °C. In both cases, in the IMC-controlled regime, the strengths overlapped because the IMC thickness was relatively constant.

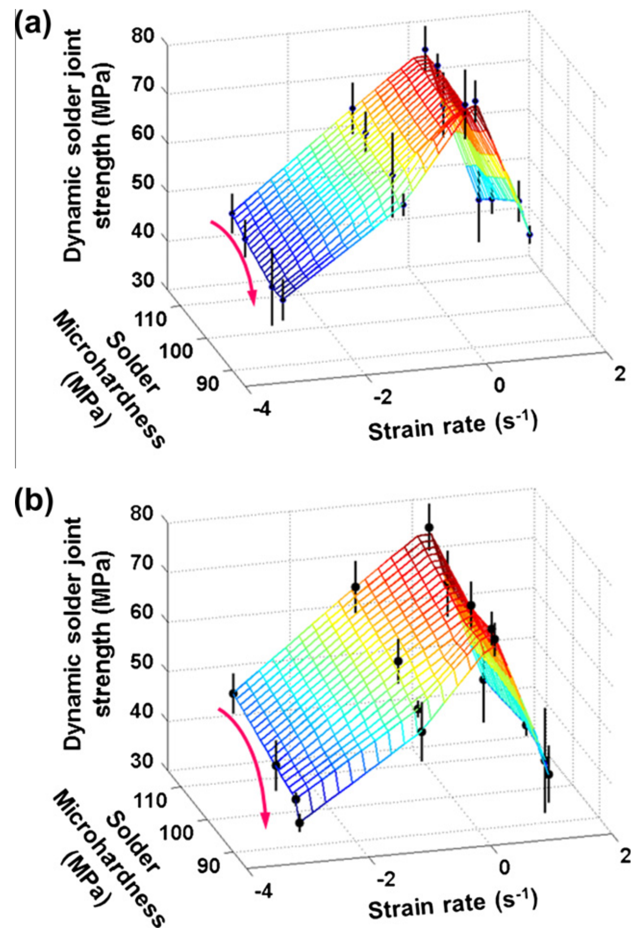

Fig. 7. 3-D visualization of dynamic solder joint strengths for joints aged at (a) 140 °C and (b) 175 °C. Dynamic solder joint strength was a continuous function of the solder microhardness, and decreased with decreasing solder microhardness. Strengths in the solder-controlled regime were greater for joints aged at 140 °C, while the strengths in the IMC-controlled regime overlapped.

the solder-controlled and IMC layer-controlled trends observed in the previous section hold true for larger IMC layers.

In this section we discuss the results on the effect of IMC thickness on mechanical shock behavior. UTS values from tensile tests conducted over a range of strain rates were plotted as a function of strain rate to show the dynamic strength of the solder joint, as shown in Fig. 8. The green curve shown in Fig. 8a is the dynamic solder joint strengths of as-reflowed solder joints, and was an experimental control against which all other trends in dynamic strength were compared. Fig. 8a shows the dynamic strengths for solder joints held in extended reflow for 3, 24, and 168 h. The average IMC layer thicknesses for as-reflowed solder joints, and solder joints held in extended reflow for 3, 24, and 168 h, were 2.5 ± 0.6 μm, 14.0 ± 5.9 μm, 22.8 ± 9.7 μm, and 44.0 ± 15.9 μm, respectively. Unlike the experiments described in the previous section, the solder microhardness was kept constant for these joints, and was equal to 113.9 ± 4.8 MPa.

An increase in IMC layer thickness caused a reduction in dynamic solder joint strength at all strain rates, due to the increase in stress concentration with strain rate in the brittle IMC layer. Some weak strain rate hardening is present for the solder joints with an IMC layer thickness of 14.0 ± 5.9 μm. At this IMC layer thickness solder-controlled and IMC layer-controlled dynamic solder joint strength regimes could still be identified, and a transition from solder-controlled to IMC layer-controlled regimes was observed at ∼1 s^{-1}. The dynamic solder joint strength decreased with increasing strain rate for solder joints with IMC layer thicknesses larger than 14.0 ± 5.9 μm.

These results are similar to those observed by Hayes et al. [43], who measured ∼28% decrease in fracture toughness, and a prevalence of brittle IMC layer fracture, when

Author's personal copy

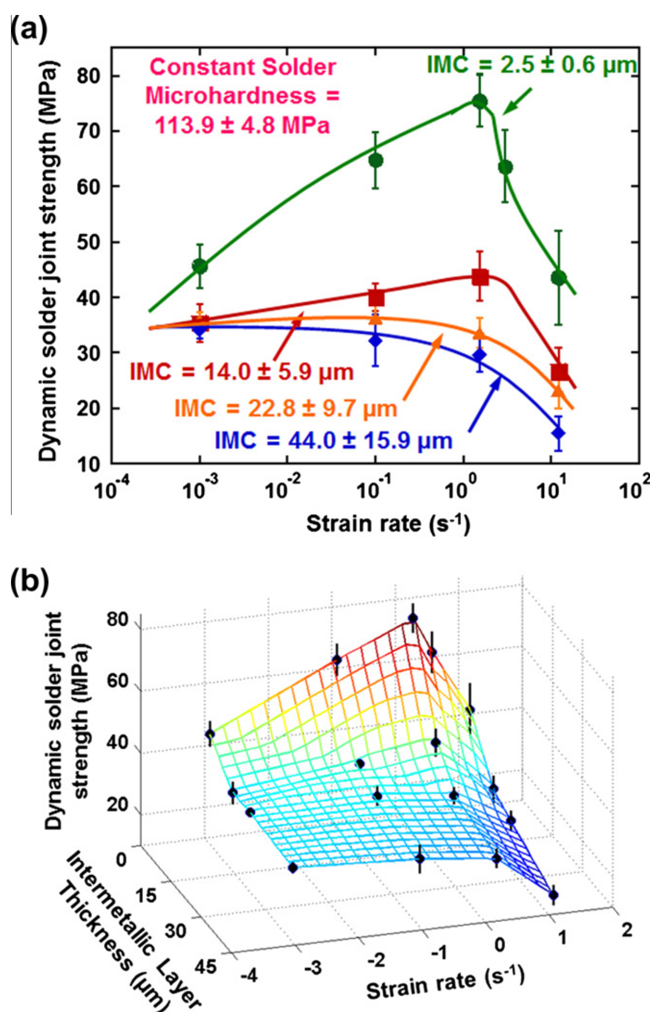

Fig. 8. (a) UTS plotted as a function of strain rate for as-reflowed and extended reflow solder joints showed the trend in solder-controlled and IMC-controlled strengths. Increase in IMC layer thickness reduced strength at all strain rates. (b) 3-D visualization of dynamic solder joint strengths for extended reflow solder joints. Dynamic solder joint strength was a continuous function of the IMC layer thickness, and decreased with increasing IMC layer thickness.

the IMC layer thickness was increased from 3 μm to 5 μm for Sn–4.0 Ag–0.5 Cu compact tension specimens. Lee et al. [42] observed predominantly cleavage fracture in Sn–3.5 Ag solder joints with IMC layer thicknesses greater than 10 μm, whereas Deng et al. [26] saw predominantly cleavage fracture in Sn–3.5 Ag solder joints with IMC layer thicknesses greater than 20 μm. The experimental results presented here indicate that a critical IMC layer thickness exists between 14 and 22 μm, at which cleavage fracture through the IMC layer becomes the dominant deformation mode. This indicates that the solder-controlled and IMC layer-controlled relationships identified in the previous section do not hold for relatively large IMC layer thicknesses. The influence of this unique dynamic solder joint strength behavior on solder joints reliability will increase as a greater number of solder interconnects are squeezed into smaller packages, because the ratio of the brittle IMC layer volume to the solder volume will increase.

The influence of the IMC layer thickness and strain rate on the dynamic solder joint strength was visualized in three dimensions. Fig. 8b shows the dynamic solder joint strength plotted as a function of IMC layer thickness and strain rate for extended reflow solder joints. It can be seen that the solder-controlled dynamic strength regime gently slopes into an almost flat plateau region for large IMC layer thicknesses. Conversely, the IMC layer-controlled dynamic strength regime rapidly begins to drop off for large IMC layer thicknesses and higher strain rates. The 3-D visualizations of dynamic solder joint strength presented so far, which depict the relationships with solder microhardness and IMC layer thickness, offer a method for optimizing the mechanical shock resistance of Sn-rich, Pb-free solder joints. For instance, by inspecting Fig. 7 one can determine the peak dynamic solder joint strength for a given solder microhardness, before which brittle IMC layer fracture takes over. Similarly, Fig. 7a and b suggests how the solder microhardness can be adjusted to tailor the dynamic solder joint strength for a given strain rate. Fig. 8b shows how rapidly the dynamic solder joint strength decreases with increasing IMC layer thickness for a given strain rate. For example, Fig. 8b suggests that decreasing the IMC layer thickness from ∼15 μm to 5 μm will improve the dynamic solder joint strength ∼33% at 1 s^{-1}, while only ∼25% improvement is gained at 10^{-2} s^{-1}.

3.4. Fractographic analysis

Solder joint fracture surfaces were examined to elucidate the relationship between fracture mechanisms and the dynamic solder joint strength. In general, fracture was observed to propagate close to the solder/copper interface for all samples, possibly due to constraint imposed by the geometry of the solder joint [39] and the propensity for the interface to serve as a site for stress concentration [28,43]. Fractographs of solder joints isothermally aged at 140 °C were organized by increasing strain rate and decreasing solder microhardness in Fig. 9a. The fracture surfaces transitioned from ductile dimple morphology to cleavage fracture with increasing strain rate. Zou and Zhang [38,39] observed a similar increase in IMC layer cleavage fracture commensurate with increasing strain rate. Kumar et al. [41] quantified the fraction of IMC layer cleavage fracture, and showed that it had a linear relationship with strain rate.

At low strain rate ductile dimple morphology of the Sn alloy was found on the fracture surface. EDS spot scans identified broken Cu_6Sn_5 nodule tips at the bottom of dimples. This indicated that voids were nucleated in the solder due to the stress concentration created by the Cu_6Sn_5 nodules, followed by crack propagation near the intermetallic layer as the voids grew and coalesced. As solder microhardness decreased, slightly larger ductile dimples were found on the fracture surface. Deng et al. [26] and Zou and Zhou [38,39] also observed that ductile dimples on the fracture surface increased in size commensurately with aging time,

Author's personal copy

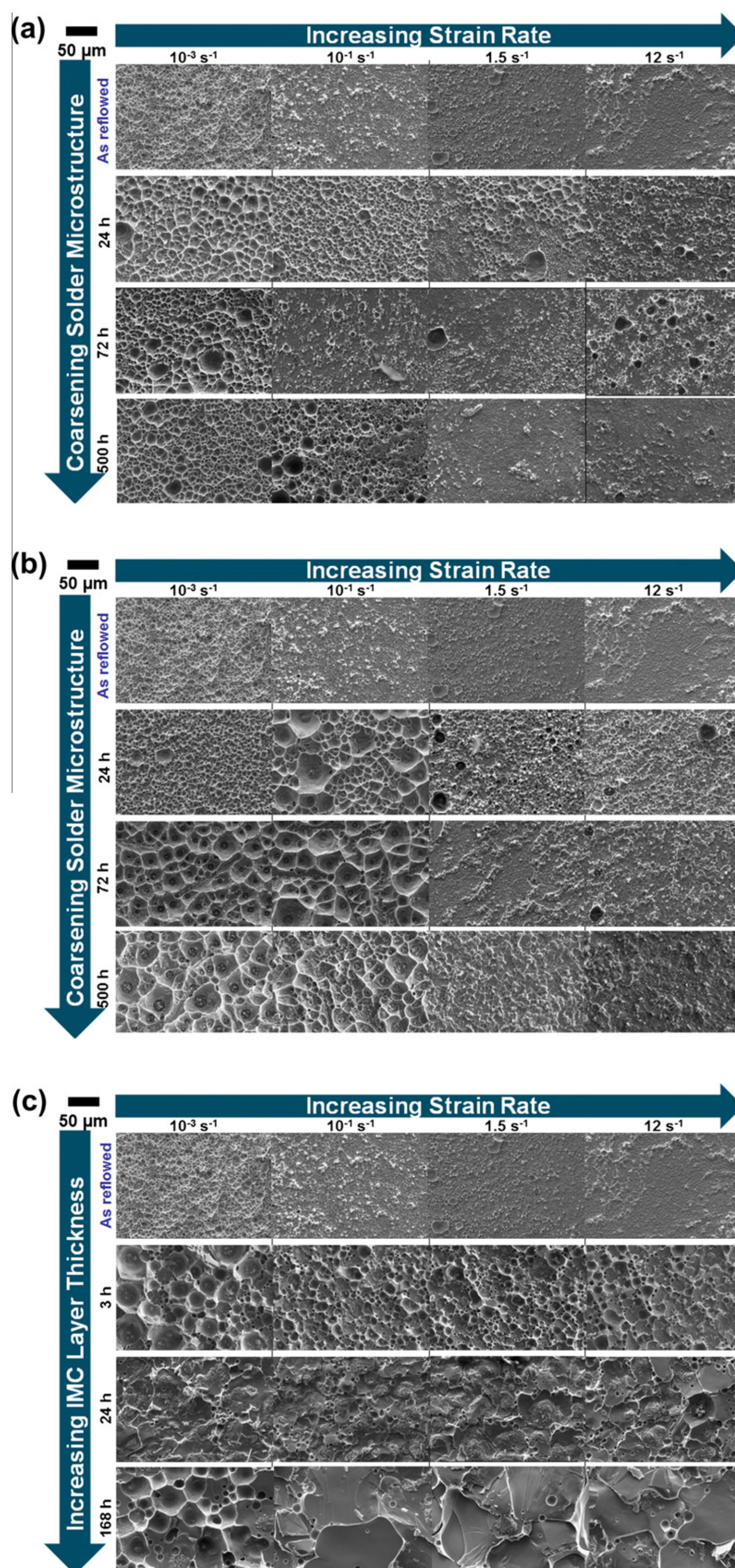

Fig. 9. Fractographs organized by increasing strain rate and coarsening solder microstructure or increasing IMC layer thickness. Fractography of solder joints isothermally aged at (a) 140 °C, (b) 175 °C showed a tendency toward brittle IMC fracture with increasing strain rate, and a prevalence of ductile dimples nucleated by Cu_6Sn_5 nodule tips with coarsening of solder microstructure. Some debonding between Cu_6Sn_5 nodules and Sn-rich matrix was noticed at intermediate strain rates and coarsening states, while some fracture between Cu_3Sn and Cu_6Sn_5 was noticed at the higher strain rates and for greater microstructure coarsening. Extended reflow solder joints tended toward brittle IMC fracture with increasing strain rate and increasing IMC layer thickness. Concurrent increases in strain rate and IMC layer thickness produced some fracture between Cu_3Sn and Cu_6Sn_5.

Author's personal copy

due to the coarsening of the solder microstructure, particularly Ag_3Sn precipitates. Therefore more plastic deformation could take place, and larger ductile dimples were nucleated for a given strain rate.

At intermediate strain rates and solder microhardnesses, fracture tended to occur at the Cu_6Sn_5 IMC layer due to an increase in stress triaxiality in the Sn-rich matrix, leaving very little time for stress relaxation, and localizing brittle fracture at the IMC layer. At the strain rate corresponding to the transition between solder-controlled and IMC layer-controlled strength, there was some ductile debonding of the Sn-rich matrix from the IMC layer. The evidence for this mode of deformation was fully exposed Cu_6Sn_5 nodules, and Cu_6Sn_5 nodule-shaped dimples on the mating fracture surface. At the transition strain rate there was some fracture through the IMC layer as well, indicating that at this strain rate both fracture mechanisms contributed to the overall strength of the joint. Hayes et al. [43] also observed the same sort of debonding of the solder matrix from the IMC layer, leaving behind intact Cu_6Sn_5 nodules in Sn–0.7 Cu and Sn–4.0 Ag–0.5 Cu solder joints. In that study as well, the fracture surface consisted of a mixture of ductile dimples and debonded solder.

Higher strain rates and lower solder microhardness promoted more IMC layer cleavage fracture. High strain rate increases solder yield strength, which builds greater stress in the IMC layer, thereby causing brittle fracture. At the highest strain rate, the fracture surface consisted of cleavage fractured Cu_6Sn_5. Little solder was found on the cleavage fracture surface, which indicated that the tensile strength of solder joints tested was controlled by the IMC layer. Kumar et al. [41] and Zou and Zhang [38,39] observed similar increases in cleavage fractured IMC layer with increasing strain rate. At the highest strain rate and lower solder microhardness (longer aging time), a small amount of debonding between Cu_3Sn and Cu_6Sn_5 in the intermetallic layer occurred. The evidence for this fracture mechanism was exposed small Cu_3Sn grains, identified by EDS spot scan, on the fracture surface. However, the Cu_3Sn layer is very thin and does not seem to affect the mechanical results.

The fracture behavior was shown to have a significant dependence on the solder microstructure, especially in the low strain rate, solder-controlled regime. Fractographs of solder joints isothermally aged at 175 °C are shown in Fig. 9b. Similar to joints aged at 140 °C, the fracture surfaces transitioned from ductile dimple morphology to cleavage with increasing strain rate. At low strain rate, ductile dimple morphology was found on the fracture surface. The dimples were larger than those formed in the joints aged at 140 °C. The larger ductile dimples are consistent with the lower solder microhardnesses for joints aged at 175 °C. Lower solder microhardness implies that more ductile deformation was able to occur, and larger ductile dimples could be nucleated for a given aging time and strain rate. Lee et al. [42] also saw that ductile dimples became larger, creating a rougher fracture surface, with increasing aging time in pure Sn solder joints.

At intermediate strain rates and solder microhardnesses, fracture tended to occur along the solder/Cu_6Sn_5 interface due to an increase in stress triaxiality in the Sn-rich matrix. At the strain rate corresponding to the transition between solder-controlled and IMC layer-controlled strength, there was some ductile debonding of the Sn-rich matrix from the IMC layer. At the transition strain rate there was some fracture through the IMC layer as well, indicating that at this strain rate both fracture mechanisms contributed to the overall strength of the joint. At the highest strain rate, the fracture surface consisted of cleavage fractured Cu_6Sn_5. Little solder was found on the cleavage fracture surface, which indicated that the tensile strength of solder joints tested was controlled by the IMC layer. At the highest strain rate and lower solder microhardness, some debonding between Cu_3Sn and Cu_6Sn_5 in the intermetallic layer occurred. In this case, the amount of debonded Cu_3Sn and Cu_6Sn_5 was slightly more than that for joints aged at 140 °C. Thus, the relationships between the dynamic strengths of solder joints, with constant IMC layer thickness and varying solder microstructure, and their fracture mechanisms were characterized.

The fracture behavior of solder joints with large IMC layer thickness differed greatly from that observed for thin IMC layers. Fractographs of extended reflow solder joints were organized by increasing strain rate and increasing IMC layer thickness in Fig. 9c. The fracture surfaces of the solder joints with IMC layer thickness = 14.0 ± 5.9 μm (3 h reflow) transitioned from ductile dimple morphology to cleavage fracture with increasing strain rate. This fracture morphology was consistent with the weak strain rate hardening observed in the dynamic solder joint strength curve. Somewhat larger ductile dimples, which were nucleated by larger IMC nodules, were found on the fracture surfaces. Hayes et al. [43] also observed increases in brittle IMC layer fracture of ~40% in Sn–0.5 Cu solder joints when the IMC layer thickness was increased from ~4 μm to ~8 μm. Solder joints with IMC layer thickness greater than 14.0 ± 5.9 μm exhibited cleavage fracture of the Cu_6Sn_5 IMC layer, indicating that the overall dynamic solder joint strength was controlled predominantly by the IMC layer. Kumar et al. [41] observed a similar increase in brittle IMC layer fracture with increasing IMC layer thickness. They reasoned that the relationship between brittle fracture and IMC layer thickness was due to the increased probability that a critical flaw size would be encountered in the larger IMC layer by a main crack. At longer reflow times and higher strain rates, some fracture between Cu_3Sn and Cu_6Sn_5 IMC layers occurred.

In summary, for solder joints with relatively thin (<10 μm) and constant IMC layer thickness the solder-controlled and IMC layer-controlled dynamic strength regimes, hypothesized in Fig. 1, are evident. In the solder-controlled regime, ductile deformation is dominant and ductile dimples are observed in fractography. In the IMC layer-controlled regime, cleavage fracture through the IMC layer dominants. At the critical transition strain

Author's personal copy

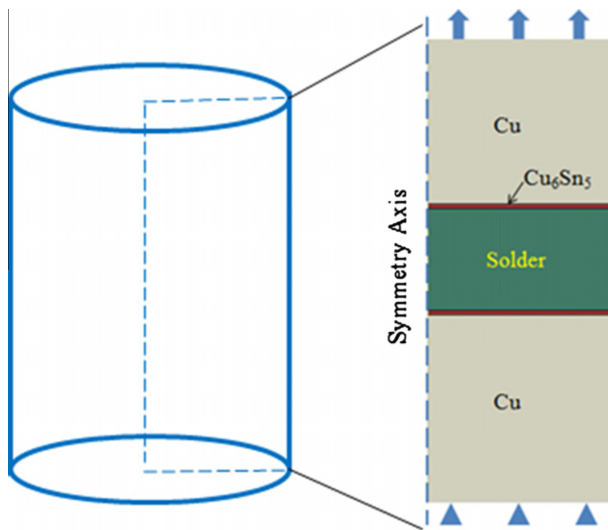

Fig. 10. Solder joint model used in finite element method simulation.

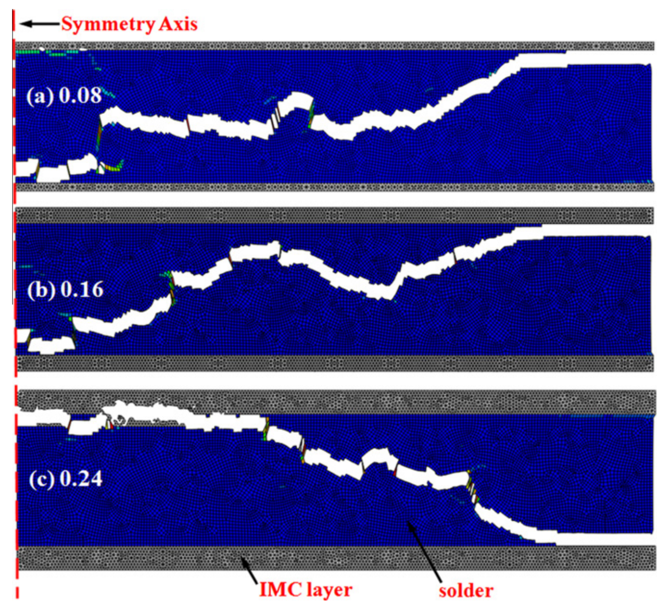

Fig. 11. Simulation of influence of IMC layer thickness on SAC solder joint fracture at 10 s^{-1}. The ratio of the IMC layer thickness to the total joint thickness was (a) 0.08, (b) 0.16, and (c) 0.24. Propensity for brittle IMC fracture increases with increasing ratio of IMC layer thickness to total joint thickness.

rate, a mixture of ductile deformation and brittle fracture occurs. Both of these mechanisms contribute to the overall dynamic solder joint strength. Coarsening of solder microstructure produces commensurately lower dynamic strengths, and larger ductile dimples in the solder-controlled regime. For solder joints with constant solder microstructure and varying IMC layer thickness, the solder-controlled and IMC layer-controlled dynamic strength regimes do not necessarily apply. Indeed, it was observed that for solder joints with IMC layer thickness $\leqslant$14 μm, some weak strain rate hardening was present, and the fracture surface transitioned from ductile dimple morphology to cleavage fractured IMC with increasing strain rate. However, for IMC layer thickness $\geqslant$14 μm the dynamic solder joint strength was reduced at all strain rates, due to the dominance of IMC layer cleavage fracture. The next section will discuss numerical simulations which accurately capture the strain-rate-dependent fracture behavior for solder joints with thin/constant IMC layer, and the volume-dependent strength exhibited by larger IMC layer thicknesses.

3.5. Modeling mechanical shock fracture behavior of Sn-rich (Pb-free) solder joints

Kumar et al. [41] reasoned that the influence of IMC layer thickness on the fracture behavior observed in their joints was due to the presence of flaws within the IMC layer. Indeed, it is well known that brittle materials, particularly ceramics, exhibit a volume dependence of strength. Larger volumes provide a greater chance of a strength-limiting flaw to be present. Clearly, the IMC layer needs to be modeled as a material with defects. However, the fracture stress of Cu_6Sn_5 used in our simulations was measured from micropillar compression of single crystal nodules [22]. We expect that the behavior of the bulk IMC layer will have a lower strength than the values

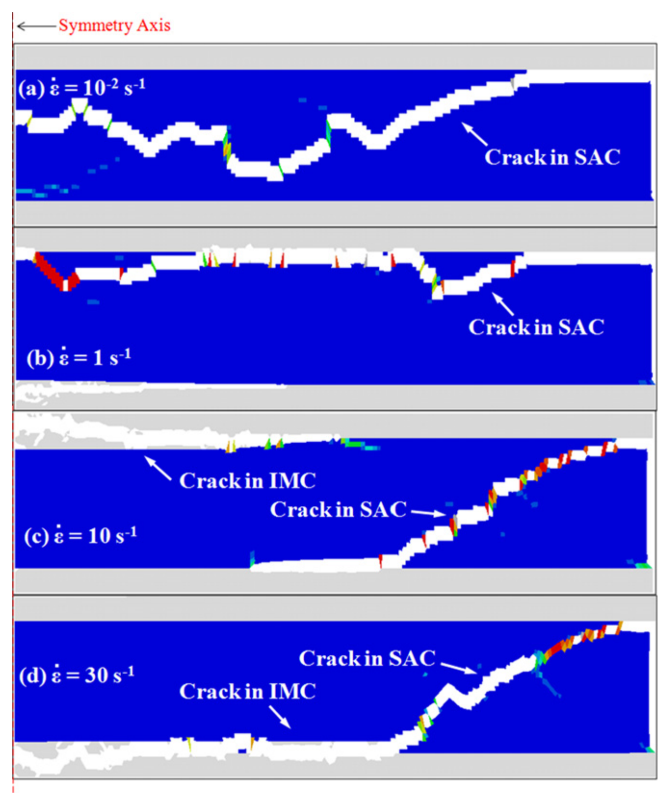

Fig. 12. Simulation of influence of strain rate on fracture behavior of SAC solder joint. The ratio of the IMC layer thickness to the total joint thickness is 0.24. The propensity for brittle IMC fracture increases with strain rate. Fracture through IMC layer is first observed at 1 s^{-1}, similar to the transition from solder-controlled to IMC layer-controlled dynamic strength observed experimentally at 1 s^{-1}.

Author's personal copy

obtained by pillar compression, because the volumes are larger and tensile stresses are a more severe loading condition for flaws in brittle solids. The volume-dependence of the IMC layer strength was introduced by modeling the IMC layer with randomly assigned defect elements. 40% of the total number of Cu_6Sn_5 elements was randomly assigned lower fracture stresses, to created flawed IMC layer elements for this finite element analysis. Empirically, a range of fracture stresses 300–600 MPa was used for the flawed elements.

The results presented so far from literature and experiment has shown that the solder joint fracture behavior is indeed influenced by the IMC layer thickness. Therefore, the results presented in this section focus on modeling the effect of IMC layer thickness, while keeping the microstructure and applied strain rate constant. The applied strain rate was $10\ s^{-1}$. In order to make the simulation results more meaningful, the ratio of the IMC layer thickness to total joint thickness (α) are reported. Three simulations were conducted, in which $\alpha = 0.08$, 0.16, and 0.24. The axisymmetric solder joint model is shown in Fig. 10.

The solder joint model was axisymmetric, and consisted of Sn–3.5 Ag–0.7 Cu solder alloy, Cu_6Sn_5 IMC layers, and copper bars. The model geometry was the same as that of the experimental joints. Perfect bonding between the copper, IMC, and solder was assumed. Copper was modeled as an elastic material with Young's modulus of 116.5 GPa, Poisson's ratio of 0.34 and density of $8.9\ g\ cm^{-3}$. The Cu_6Sn_5 IMC layer was modeled with a Young's modulus of 112 GPa, Poisson's ratio of 0.3, density of $8.3\ g\ cm^{-3}$, yield strain of 1.2%, fracture stress $\sim$1350 MPa, and failure strain of 1.37%. The mechanical properties of the Cu_6Sn_5 IMC layer were obtained from in situ compression measurements on micropillars [22]. The solder was modeled as a plastic material, with Young's modulus of 51 GPa, Poisson's ratio of 0.3, and density of $7.37\ g\ cm^{-3}$. Fracture resulted from the void nucleation, growth, and coalescence. The elements next to the interface were allowed to fracture. Tensile displacement rate was applied to maintain a nominal strain rate. Additional details of the finite element analysis are available elsewhere [27,28].

The influence of the IMC layer thickness on the solder joint fracture behavior is shown in Fig. 11. The solder is shown in blue, the IMC layer is gray, and the fractured region is white. In Fig. 11a, the IMC layer was relatively thin ($\alpha = 0.08$), and the cracks were mostly confined to the solder region. When α was increased to 0.16, as in Fig. 11b, fracture occurred in the IMC layer. Similar to the experimental results, we see that when the IMC layer was relatively thin, ductile deformation dominated. As the IMC layer thickness increased the simulation showed that there was a greater probability that the IMC layer would serve as a crack initiation site, thereby decreasing the dynamic solder joint strength and initiating more IMC layer cleavage fracture.

The experimental results have shown that solder joint fracture behavior is also influenced greatly by the strain rate. Here, the influence of strain rate is discussed. α was fixed at 0.24, and the strain rate was varied from $10^{-2}\ s^{-1}$ to $30\ s^{-1}$. The strain-rate-dependent simulation results are shown in Fig. 12. Fracture initiated in the solder at low strain rate, as shown in Fig. 12a. This fracture behavior is similar to the solder-controlled dynamic solder joint strength regime verified experimentally. When the strain rate was increased to $1\ s^{-1}$, fracture began to take place in the IMC layer. This fracture behavior may correspond to the transition between solder-controlled and IMC layer-controlled dynamic solder joint strength, as shown in Fig. 12b. Fig. 12c shows that as the strain rate was increased to $10\ s^{-1}$, fracture began to occur in both the solder and IMC layer. At $30\ s^{-1}$, the length of fractured IMC layer is greater than half the total fracture length, which is similar to the IMC layer-controlled dynamic solder joint strength regime.

The dominant fracture behavior, i.e. solder-controlled or IMC layer-controlled, is a result of the competition between stress relaxation in the solder and brittle fracture at the IMC layer. Cu_6Sn_5 is certainly much stiffer than SAC solder, and has a much lower strain-to-failure. The experimental and simulation results have shown that at low strain rates, the solder yields, and ductile fracture takes place before fracture can occur in the IMC layer. However, at higher strain rates the solder cannot relax and a state of high stress triaxiality builds up within the solder. The high stress triaxiality may overcome the fracture stress of the IMC layer, thereby initiating brittle fracture in the IMC layer, particularly at microscopic flaws.

4. Conclusions

The behavior of Sn alloy–Cu couples was investigated over a variety of solder strengths, IMC thickness, and strain rate. The following important points were derived from this study:

- The hypothesized behavior shown in Fig. 1, consisting of solder-controlled and IMC layer-controlled strength regimes was experimentally verified over a range of strain rates. However, this behavior only applies to the case where the IMC thickness is relatively thin. At higher IMC thickness (>15 μm), IMC fracture controls the deformation behavior at all strain rates.
- At low IMC thickness, a decrease in solder strength, with a constant IMC layer thickness, produced a commensurate decrease in the dynamic solder joint strength in the solder-controlled regime. In the IMC layer-controlled regime the dynamic strengths overlapped. An increase in IMC layer thickness, with a constant solder microhardness, reduced dynamic solder joint strength at all strain rates.

Author's personal copy

- Fracture mechanisms in solder joints with constant IMC layer thickness and varying solder microstructure were elucidated. In the solder-controlled strength regime ductile dimple fracture morphology was observed. In the IMC layer-controlled strength regime cleavage fracture of the Cu_6Sn_5 IMC layer was observed. At the critical strain rate corresponding to the transition from solder-controlled to IMC layer-controlled strength there was a mixture of ductile debonding of the Sn-rich matrix from the Cu_6Sn_5 IMC layer, and cleavage fracture of the Cu_6Sn_5 IMC layer, indicating that both ductile solder deformation and brittle IMC fracture contributed to the overall dynamic solder joint strength.
- Fracture mechanisms in solder joints with constant solder microstructure and varying IMC layer thickness were elucidated. Solder joints with moderately thick IMC layer ($\leqslant$14 μm) transitioned from ductile dimple morphology to cleavage fracture with increasing strain rate. Solder joints with large (>14 μm) IMC layer thickness tended fracture by cleavage through the IMC at all strain rates. Therefore, we see that the solder-controlled and IMC layer-controlled strength regimes do not necessarily apply for joints with large IMC layer thickness.
- Finite element analysis was conducted to study the influences of IMC layer thickness and strain rate on the fracture behavior of solder joints. The finite element results agreed well with the experimentally observed fracture behavior. Larger IMC layer thicknesses showed a propensity for brittle fracture. The volume-dependent strength was incorporated into the model to accurately simulate the fracture behavior. As the strain rate increased, the fracture behavior transitioned from ductile to brittle. The onset of brittle fracture in the IMC layer was at $\sim 1\ s^{-1}$, similar to the experimentally observed behavior.

Acknowledgments

The authors are grateful for the financial support for this work from the National Science Foundation Division of Materials Research – Metals Division (Drs Alan Ardell, Bruce MacDonald, and Harsh Chopra, Program Directors). The authors gratefully acknowledge the use of facilities within the Leroy Eyring Center for Solid State Science at Arizona State University. The assistance of Dr Jason Williams with mechanical testing is appreciated.

References

[1] Chawla N. Int Mater Rev 2009;54:368.
[2] Glazer J. JEM 1994;23:693.
[3] Glazer J. Int Mater Rev 1995;40:65.
[4] McCormack M, Jin S. JOM 1993;45:36.
[5] Vianco PT, Frear DR. JOM 1993;45:14.
[6] Plumbridge WJ. J Mater Sci 1996;31:2501.
[7] Tee TY, Ng HS, Lim CT, Pek E, Zhong Z. Microelectron Reliab 2004;44:1131.
[8] Reiff D, Bradley E. IEEE Elec Comp C Proc 2005;55:1519.
[9] Date M, Shoji T, Fujiyoshi M, Sato K, Tu KN. IEEE Elec Comp C Proc 2004;54:668.
[10] Tsai KT, Liu FL, Wong EH, Rajoo R. Solder Surf Mt Tech 2006;18:12.
[11] Pandher P, Boureghda M. Int Rel Phys Proc 2007;45:107.
[12] Newman K. IEEE Elec Comp C Proc 2005;55:1194.
[13] Chia JY, Cotterell B, Chai TC. Mat Sci Eng A 2006;417:259.
[14] Ochoa F, Williams JJ, Chawla N. JOM 2003;55:56.
[15] Ochoa F, Deng X, Chawla N. JEM 2004;33:1596.
[16] Darveaux R, Reichman C. IEEE El Packag Tech Conf Proc 2006;8:283.
[17] Fei H, Yazzie K, Williams J, Chawla N, Jiang H. J Comput Theor Nanos 2011;8:873.
[18] Wong EH, Rajoo R, Mai YW, Sean SK, Tsai KT, Yap LM. IEEE Elec Comp C Proc 2005;55:1202.
[19] Yazzie KE, Williams JJ, Kingsbury D, Peralta P, Jiang H, Chawla N. JOM 2010;62:16.
[20] Mattila TT, Kivilahti JK. JEM 2005;34:969.
[21] Deng X, Koopman M, Chawla N, Chawla K. Mat Sci Eng A 2004;364:240.
[22] Jiang L, Chawla N. Scripta Mater 2010;63:480.
[23] Yazzie K, Xie H, Williams J, Chawla N. Scripta Mater 2012;66:586.
[24] Geng P, Chen P, Yun Ling. IEEE Elec Comp C Proc 2002;52:974.
[25] Suh D, Kim DW, Liu P, Kim H, Weninger JA, Kumar CM, et al. Mat Sci Eng A 2007;460–461:595.
[26] Deng X, Sidhu R, Johnson P, Chawla N. Metall Mater Trans A 2005;36:55.
[27] Fei H, Yazzie KE, Chawla N, Jiang H. J Comput Theor Nanos 2011;8:873.
[28] Fei H, Yazzie, KE, Chawla, N, Jiang, H. JEM, in press.
[29] Yazzie K, Topliff J, Chawla N. Metall Mater Trans 2012, submitted for publication.
[30] Chawla N, Shen YL, Deng X, Ege ES. JEM 2004;33:1589.
[31] Deng X, Chawla N, Chawla KK, Koopman M. Acta Mater 2004;52:4291.
[32] Stepniak F. Microelectron Reliab 2004;44:805.
[33] Wong EH, Rajoo R, Mai YW, Seah SKW, Tsai KT, Yap LM. IEEE Elec Comp C Proc 2005;55:1202.
[34] Zaal JJM, Hochstenbach HP, van Driel WD, Zhang GQ. Microelectron Reliab 2009;49:846.
[35] Lal A, Bradley E. IEEE Elec Comp C Proc 2006;56:1628.
[36] Darveaux R, Reichman C. IEEE Elec Comp C Proc 2006;56:283.
[37] Su YA, Tan LB, Tee TY, Tan VBC. Microelectron Reliab 2010;50:564.
[38] Zou HF, Zhang ZF. J Mater Res 2008;23:1614.
[39] Zou HF, Zhang ZF. Microelectron Eng 2010;87:601.
[40] Huang Z, Kumar P, Dutta I, Pang JHL, Sidhu R, Renavikar M, et al. JEM 2012;41:375.
[41] Kumar P, Huang Z, Dutta I, Sidhu R, Renavikar M, Mahajan R. JEM 2012;41:412.
[42] Lee HT, Chen MH, Jao HM, Liao TL. Mater Eng A 2003;358:134.
[43] Hayes SM, Chawla N, Frear DR. Microelectron Reliab 2009;49:269.